HOKKAIDO UNIVERSITY

Title	The solid-phase partitioning of arsenic in unconsolidated sediments of the Mekong Delta, Vietnam and its modes of release under various conditions
Author(s)	Dang Thuong Huyen; Tabelin, Carlito Baltazar; Huynh Minh Thuan et al.
Citation	Chemosphere, 233, 512-523 https://doi.org/10.1016/j.chemosphere.2019.05.235
Issue Date	2019-10
Doc URL	https://hdl.handle.net/2115/82845
Rights	© 2019. This manuscript version is made available under the CC-BY-NC-ND 4.0 license https://creativecommons.org/licenses/by-nc-nd/4.0/
Rights(URL)	https://creativecommons.org/licenses/by-nc-nd/4.0/
Type	journal article
File Information	Manuscript (Chemosphere-revision 1).pdf

Hokkaido University Collection of Scholarly and Academic Papers : HUSCAP

The solid-phase partitioning of arsenic in unconsolidated sediments of the Mekong Delta, Vietnam and its modes of release under various conditions

Dang Thuong Huyen[a], Carlito Baltazar Tabelin[b,] *, Huynh Minh Thuan[a], Dang Hai Dang[a], Phan Thi Truong[a], Banthasith Vongphuthone[c], Masato Kobayashi[c], and Toshifumi Igarashi[d]

[a] Environmental Geology Department, Faculty of Geology and Petroleum Engineering, Ho Chi Minh City University of Technology, 168 Ly Thuong Kiet, Dist. 10, HCMC, VIETNAM

[b] School of Minerals and Energy Resources Engineering, The University of New South Wales, Sydney, NSW 2052, AUSTRALIA

[c] Division of Sustainable Resources Engineering, Graduate School of Engineering, Hokkaido University, JAPAN

[d] Division of Sustainable Resources Engineering, Faculty of Engineering, Hokkaido University, JAPAN

Abstract

Arsenic (As) contamination of the groundwater in the Mekong Delta is a serious problem affecting millions of people who rely on this important resource for drinking and agriculture. In this study, borehole cores up to a depth of 40 m were collected in the Vietnamese-side of the delta and the solid-phase partitioning of As with depth was investigated to understand the factors and processes controlling its release under oxic, acidic and reducing conditions. The results showed that in most of the sediments, substantial amounts of As are partitioned with exchangeable phases that are easily released into solution. Two borehole cores obtained between the Hau and Tien Rivers also had significantly high As partitioned with organic/sulfide phases and one of these cores had abundant As-bearing pyrite in 1-m thick peat layers. Leaching experiments in deionized (DI) water coupled with principal component analysis suggest that As release is controlled by sorption-desorption reactions with clays/phyllosilicates (i.e., kaolinite, muscovite and clinochlore), proton-promoted dissolution of iron-oxyhydroxides, and oxidation of pyrite/organic matter. The release of As was further promoted under acidic conditions in the presence of chloride (Cl^-), which suggests that seasonal drying/flooding episodes generating acid sulfate soils, as well as salt water intrusion due to excessive groundwater abstraction may exacerbate this problem in the future.

Keywords: Vietnamese Mekong Delta; arsenic; leaching; sequential extraction; pyrite; phyllosilicates

*Corresponding author: Tel: +61 (02) 9385 7946

Email: c.tabelin@unsw.edu.au; carlito.tabelin@gmail.com

1. INTRODUCTION

Groundwater contaminated with arsenic (As) is one of the biggest and most serious health threats in developing countries because it is almost always used directly without prior treatment (Smedley and Kinniburgh, 2002). Arsenic is a metalloid with mutagenic, carcinogenic and teratogenic properties, and prolonged exposure to it even in minute amounts (i.e., chronic poisoning) via ingestion of contaminated drinking water could cause arsenicosis, Blackfoot disease and the higher risks of developing various types of cancers (Tabelin et al., 2018). To date, As-contaminated groundwater has been reported in over 70 countries and is affecting more than 150 million people worldwide (Ravenscroft et al., 2009).

The Mekong Delta, situated in Cambodia and Vietnam, is an important aquifer system with prevalent and serious As-contaminated groundwater problem. The delta plain was formed as the Mekong River breaks into several arteries before reaching the sea and has an area of around 62 000 km^2 with about 84% of it situated in Vietnam while the rest is in Cambodia (~16%) (Nguyen et al., 2000). Arsenic contamination of groundwater in the Mekong Delta was first reported in 2001 by a study conducted in Cambodia (Feldman and Rosenboom, 2001). Six years later, Berg and coworkers (2007) reported that groundwater in the Vietnamese-side of the Mekong Delta was also contaminated with As. They further estimated that more than 17 million Vietnamese living on the delta is highly at risk of chronic As poisoning. In fact, the hairs of some affected Vietnamese already had elevated As levels, an early symptom of chronic As poisoning (Berg et al., 2007). With the rapid population increase in this region coupled with the extensive use of groundwater for drinking and agriculture, this As-contaminated groundwater problem will likely worsen as observed in other parts of the world like Bangladesh and West Bengal, India with high population densities (Fendorf et al., 2010; Harvey et al., 2002).

The geological, hydrological and biological processes crucial in the release of As to groundwater as well as its migration through aquifer systems are increasingly becoming well defined in recent years. Polizzotto and coworkers (2008), for example, studied in detail how hydrological and biogeochemical conditions affected As fluxes in a minimally disturbed area of the Mekong Delta in Kandal Province, Cambodia and found that wetlands and near-surface sediments supplied As to lower

regions of the aquifer. A follow-up paper by these authors proposed that organic matter from wetlands was likely co-deposited with As-bearing iron-oxyhydroxides and as these phases moved downwards into the aquifer during burial, microbial-mediated processes driven by organic matter decomposition promoted reducing conditions that remobilized As into groundwater in the deeper parts of the aquifer (Kocar et al., 2008). These studies were, however, limited in Cambodia and the area selected had a relatively simple vertical lithofacies composed mainly of an upper layer of clay and a lower layer of sand. Moreover, these studies only determined the solid-phase partitioning of As in a very shallow part of the aquifer (about 4 m from the surface). On the Vietnamese-side of the Mekong Delta, only the work of Hoang and coworkers (2010) evaluated the solid-phase partitioning of As in the sediments by sequential extraction using sections from two borehole cores. These authors provided compelling evidence that As concentration in groundwater tended to increase when the wells are closer to the Tien River, one of the main arteries of the Mekong River in Vietnam. Moreover, they reported that amorphous iron-oxyhydroxides were the primary sources of As in the sediments. Unfortunately, these authors ignored the effects of pyrite/organic matter and clay/phyllosilicate minerals likely because the sequential extraction method they employed was designed to quantify As in both amorphous and crystalline iron-oxyhydroxide/oxide phases (Silveira et al., 2006). In other words, the solid-phase partitioning of As in the sediments of the Mekong Delta still remains unclear.

Another important issue that is still not well understood is how the seasonal changes in aquifer conditions (i.e., oxidizing-reducing and acidification) affect the mobility of As in the sediments of the Mekong Delta. The climate in this region is monsoonal humid and tropical (27–30°C) with a mean annual precipitation of 1500–2400 mm, the bulk of which is delivered during the rainy season from April to November (Pham et al., 2002). These seasonal cycles of dry and wet conditions have been reported to strongly affect redox conditions in the shallow regions of the Mekong Delta including areas near the Mekong River and its tributaries (Polizotto et al., 2008). Meanwhile, the abundance of acid sulfate soils in the region suggests that acidification of sediments in the aquifer could occur as a result of hydrological changes caused by excessive groundwater abstraction or flooding/inundation episodes due to the delta's low elevation (0–4 m above sea level) (Berg et al., 2007; Nguyen and Itoi, 2009).

The above-mentioned issues are addressed in this study by providing a better understanding of the solid-phase partitioning of As in naturally contaminated aquifer sediments and the roles played by these As-bearing phases on the release of As under oxic, reducing and acidic conditions. Specifically, this study aims to: (1) determine the solid-phase partitioning of As with depth in the upper region (< 40 m) of the Vietnamese-side of the Mekong Delta, (2) investigate the effects of oxic, reducing and acidic conditions on the release of As into solution, and (3) identify the important factors and processes responsible for the mobilization/immobilization of As under various environmentally relevant conditions. The first objective was achieved by extensive characterization of the sediments using X-ray powder diffraction (XRD), X-ray fluorescence spectroscopy (XRF), scanning electron microscopy with energy dispersive X-ray spectroscopy (SEM-EDX) and sequential extraction. The second and third objectives were accomplished by batch-type leaching experiments under oxic, reducing and acidic conditions supplemented by multivariate statistical analysis and geochemical modeling.

2. MATERIALS AND METHODS

2.1 Borehole core sampling and characterization of sediments

The Mekong River breaks into two main arteries, the Tien and Hau Rivers, as it enters Vietnam and further branches out into eight smaller Rivers before reaching the sea (Hoang et al., 2010). The Vietnamese-side of the Mekong delta covers an area of around 39 200 km^2 and is composed of Holocene alluvial sediments (depths of 8–40 m) overlying late Pleistocene sediments (50–80 m) (Bui et al., 2005). Six borehole cores were drilled with depths of 20–40 m near the two main arteries of the Mekong River in Vietnam: two along the Hau River (PH and P-Hu), two near the Tien River (TT and TL), and two adjacent to river tributaries between the Hau and Tien Rivers (LS and PT) (Fig. 1). A total of 34 samples were obtained from distinct lithological features of the six borehole cores and a brief description of each sample is summarized in Supplementary Table 1. The samples were air-dried in the laboratory, sealed in polypropylene (PP) bottles, and then shipped to Hokkaido University, Japan for the detailed characterization of the sediments, leaching experiments and sequential extraction.

Prior to the chemical and mineralogical analyses, the samples were ground with an agate mortar to < 50 μm and then analyzed by XRD (MultiFlex, Rigaku Corporation, Japan) and XRF (SpectroXepos, Rigaku Corporation, Japan). Both XRD and XRF measurements were done on pressed powders of the samples. All 34 XRD patterns were also analyzed using Match!® (Crystal Impact, Germany) to identify minerals and semi-quantitatively determine their relative abundances in the samples. Loss on ignition (LOI) was determined by gravimetry; that is, a known amount of sample was heated in a muffle furnace at 750°C for 1 h after drying at 110°C in an oven for 24 h, and its loss in mass corresponded to LOI. Total organic carbon (TOC) was calculated from the total carbon (TC) and inorganic carbon (IC) contents of the sediments, both of which were measured using a total carbon analyzer attached to a solid sample combustion unit (TOC-V_{CSH}-SSM-5000A, Shimadzu Corporation, Japan). Selected samples that have exceptionally high As were also examined using SEM-EDX (Superscan SSX-550, Shimadzu Corporation, Japan).

The sequential extraction procedure used in this study was developed by Marumo and coworkers (2003) for contaminated soils and sediments based on the earlier works of Tessier et al. (1979) and Clevenger (1990). This procedure involves the sequential leaching of 1 g of sample with various lixiviants to target specific As-bearing phases. The extracted phases, lixiviants and conditions used in each extraction step are detailed as follows:

- Step 1 (exchangeable): 1 M sodium dihydrogen phosphate (NaH_2PO_4) (pH 5; 1 h; liquid-to-solid ratio of 20; 25°C; 120 rpm),
- Step 2 (carbonates): 1 M sodium acetate (CH_3COONa) (pH 5; 5 h; liquid-to-solid ratio of 20; 25°C; 120 rpm),
- Step 3 (Fe-Mn oxides): 0.04M $NH_2OH{\cdot}HCl$ in 25% acetic acid (5 h; liquid-to-solid ratio of 20; 80°C; 120 rpm), and
- Step 4 (organic and sulfides): 0.04M $NH_2OH{\cdot}HCl$ in 25% acetic acid + 30% H_2O_2 + 0.02 M HNO_3 (5 h; liquid-to-solid ratio of 36; 80°C; 120 rpm).

The residue from each extraction step was washed with 10–15 ml DI water and this solution was combined with the leachate of the extraction step and diluted to 50 ml. Finally, the residual fraction

was calculated by subtracting the total As extracted by the four steps to the As content of the sample measured by XRF.

2.2 Batch-type leaching experiments

Three types of batch-type leaching experiments were conducted in this study using a particle size of < 2 mm. Under oxic conditions, As release was evaluated by leaching 15 g of sediment samples with 150 ml of DI water at 200 rpm for 6 h using a reciprocal shaker. This method was based on the standard Japanese leaching test for contaminated soils (Environmental Agency of Japan Notification No. 46) (Tabelin et al., 2014a). After 6 h, the temperature, pH, redox potential (Eh) and electrical conductivity (EC) of suspensions were measured. Separation of liquid (supernatant) and solid (residue) was done by centrifugation for 30 min at 3500 rpm and the supernatant was filtered through 0.45 μm Millex® membrane filters (Merck Millipore, USA). The leaching experiments under reducing conditions were conducted using sodium dithionite ($Na_2S_2O_4$) as a reducing agent. Five grams of the sample (< 2 mm) were mixed with 50 ml of 0.1 M $Na_2S_2O_4$ solution at 200 rpm in a sealed 50-ml centrifuge tube to minimize the oxidation of $S_2O_4^{2-}$. After 6 h, the temperature, pH and Eh were measured and the leachates were then collected by filtration through 0.45 μm Millex® membrane filters. The leaching experiments under acidic conditions were done using hydrochloric acid (HCl) solutions. In these experiments, 3 grams of sample (< 2 mm) were mixed with 100 ml of 1 M HCl solution at 200 rpm. After 2 h, the leachates were collected by filtration of the suspension through 0.45 μm Millex® membrane filters.

2.3 Chemical analyses

Dissolved concentrations of iron (Fe), manganese (Mn), silicon (Si) and aluminum (Al) were analyzed using an inductively coupled plasma atomic emission spectrometer (ICP-AES, ICPE-9000, Shimadzu Corporation, Japan) while major coexisting cations (Ca^{2+}, Mg^{2+}, Na^{+} and K^{+}) and anions (Cl^{-}, NO_3^{-} and SO_4^{2-}) were quantified by ion chromatography (ICS-90 and ICS-1000, Dionex Corporation, USA). Dissolved As concentrations greater than 0.1 mg/l were analyzed directly by ICP-AES while leachates with less than 0.1 mg/l of As were first pretreated and then analyzed using an ICP-AES connected to a hydride-vapor generation unit (detection limit: 0.1 μg/l). For the pretreatment of

leachates with As concentrations less than 0.1 mg/l, 10 ml of the leachate sample was mixed with 5 ml of 12 M HCl, 0.67 ml of 20% potassium iodide (KI) solution, 0.67 ml of DI water, and 0.33 ml of 10% ascorbic acid solution, and this mixture was allowed to equilibrate for 3 h prior to the chemical analyses (Tabelin et al., 2013). Dissolved organic carbon (DOC) was measured by a total carbon analyzer (TOC-V_{CSH}, Shimadzu Corporation, Japan) while HCO_3^- concentrations were estimated from the alkalinity and pH using PHREEQC (Parkhurst and Appelo, 1999). The alkalinity was measured by titration of a known volume of leachate with 0.02 N sulfuric acid (H_2SO_4) solution until pH 4.8 (Eang et al., 2018a, b). The margins of error of the standard ICP-AES and ion chromatography were around 2% while the more sensitive hydride-vapor generation method for very low As concentrations had an uncertainty of about 5%.

2.4 Geochemical modeling and multivariate statistical analysis

PHREEQC was used to calculate saturation indices of some important minerals in the leaching experiments while the speciation diagram of As was created by the Geochemist's Workbench® (Bethke and Yeakel, 2011) using actual solute activities. For data interpretation, principal component analysis (PCA) was employed using Origin Pro® (OriginLab Corporation, USA). PCA is a multivariate statistical method especially useful in finding correlations in very complex systems where several components must be considered at the same time (i.e., high-dimensional data). This method simplifies the complexity of high-dimensional data while retaining trends and patterns by transforming the data into fewer “dimensions” or “summaries of features” that are called principal components (PC) (Abdi and Williams, 2010). In this study, PCA was applied to sediment samples (11 parameters of 34 samples) and leachates obtained from the leaching experiments in DI water (16 parameters of 34 samples) to give additional insights into the solid-phase phase partitioning of As and the factors and processes important in the release of this element into solution.

3. RESULTS AND DISCUSSION

3.1 Distinct lithological features of the sediments and their chemical and mineralogical compositions

Among the six borehole cores, those drilled in An Giang province located between the two rivers (LS and PT) had layers containing exceptionally high As (Fig. 2; Supplementary Figs. 1 and 2). The vertical lithofacies of these two borehole cores are composed of alternating layers of clayey silt and fine sand (Fig. 2; Supplementary Table 1) and were mainly composed of SiO_2, Al_2O_3 and Fe_2O_3 with minor amounts of MgO, CaO and K_2O. The XRD patterns and their semi-quantitative analysis of mineral abundances showed that quartz (SiO_2) (39–83%) is the dominant mineral in the sediment samples from LS and PT with moderate to minor amounts of anorthite ($CaAl_2Si_2O_8$) (2–20%) as well as moderate to trace amounts of muscovite $(K, Al)_2(AlSi_3O_{10})(FOH)_2$ (up to 23%), clinochlore $(Mg, Fe)_5Al(Si_3Al)O_{10}(OH)_8$ (up to 16%) and kaolinite ($Al_2Si_2O_5(OH)_4$) (up to 15%) (Fig. 3). Some of the sediments in LS and PT also contain gypsum ($CaSO_4 \cdot 2H_2O$) and trace amounts of calcite, dolomite, pyrite, goethite and hematite (Supplementary Tables 3). Moreover, two peat layers about 1-m thick between depths of 15 and 25 m were observed in PT and were not present in the other five borehole cores. These peat layers had lower quartz (44–46%), higher kaolinite (14–16%), more abundant TOC (about 10%) and exceptionally high As contents (~33 mg/kg).

In contrast, the As content of sediments in borehole cores collected upstream of the Hau River (Ph and P-Hu) and downstream of the Tien River (TL and TT) were all less than 20 mg/kg (Fig. 1; Supplementary Figs. 1 and 2). The geological units upstream observed in Ph and P-Hu were also very similar to that discussed earlier for LS and PT; that is, the vertical lithofacies are composed of alternating strata of clayey silt and fine sand (Fig. 2; Supplementary Fig. 1). In comparison, TL and TT had simpler vertical lithofacies than those collected upstream and were composed of coarser sediments (i.e., fine to coarse sand) (Supplementary Fig. 2). In TT, for example, fine to coarse sands were distributed from a depth of 5 to 40 m. It is interesting to note that in all borehole cores, SiO_2 and quartz increased as the particles became coarser while as the sediments became finer, the relative abundances of kaolinite, muscovite and clinochlore increased (Supplementary Tables 2–4).

PCA was used to extract important and inter-correlated dependent variables from the chemical properties of the sediments using 11 variables (SiO_2, Al_2O_3, Fe_2O_3, MgO, CaO, Na_2O, K_2O, S, As, TOC and LOI) from 34 samples (Supplementary Table 5). The results showed that three PCs had eigenvalues > 1, and they accounted for 82.9% of the total “inertia” of the composition of sediments.

PC 1 (49.07%) had high loadings of Al_2O_3, Fe_2O_3, MgO, K_2O, As and TOC, which relates the As content of sediments to clay and phyllosilicate minerals, Fe-bearing minerals, organic matter and carbonates. This means that most of As are closely associated with these minerals and phases found in the sediments, a generalization that will be discussed in more detail in the next subsection. Meanwhile, PC 2 (24.37%) and PC 3 (9.47%) could be related to the depositional processes that occurred during the delta's formation that include submersion in seawater and dolomite deposition under organic-rich environments (Supplementary information).

3.2 Solid-phase partitioning of As and its mobility under oxic, acidic and reducing conditions

The solid-phase partitioning of As in sediments from the six borehole cores and the leaching behavior of As with depth under oxic, acidic and reducing are illustrated in Fig. 4 and Supplementary Figs. 3 and 4. Leachability, L_i (mg/kg or μg/kg), was used instead of concentration to normalize the results because the weight of samples and volume of leachants used in the three types of leaching experiments were slightly different (Tamoto et al., 2015; Tabelin et al., 2017a). It was calculated as

$$L_i = \frac{C_{As} * V_L}{M_s} \quad (1)$$

where C_{As} is the concentration of As in the leachate, V_L is the volume of leachant, and M_s is the mass of sample used in the leaching experiments.

Sediments collected between the Tien and Hau Rivers (LS and PT) had substantially higher amounts of As partitioned with the organic/sulfides fraction compared with the other borehole core samples (Figs. 1 and 4; Supplementary Figs. 3 and 4). In LS, for example, As associated with the organic/sulfide phase accounted for 25–41% of the total As content of the sediments. Arsenic found with the exchangeable fraction was also substantial (13–30%) while those associated with Fe-Mn oxides and carbonates were quite low at 3–7% and 1–3%, respectively. Among the sediment samples, those from the peat layers in PT had the highest As associated with the exchangeable (~9 mg/kg) and organic/sulfide (10–12 mg/kg) phases, the sum of which was even higher than the total As content of the other samples. There are three possible explanations for this exceptionally high As in the exchangeable and organic/sulfide fractions of sediments from the peat layers. First, organic particles in these layers contained substantial amounts of As-bearing framboidal and euhedral pyrite (Figs. 5 and

6). Framboidal pyrite is typically formed in the anoxic-oxic sediment interface of estuarine systems, ancient marshlands and shallow seas when both the supply of organic carbon and the rate of sulfate reduction are low while single euhedral pyrite crystals are formed when organic matter is rich and sulfate reduction is rapid (Berner, 1984; Goldhaber and Kalan, 1974; Howarth and Teal, 1979; Rickard, 1975; Tabelin et al., 2012a). Second, As is known to strongly adsorb to organic matter like peat, lignite and coal (Besold et al., 2018; Mar et al., 2013; Wang and Mulligan 2006). Third, soluble salt-like phases, kaolinite, muscovite and clinochlore, which are known to incorporate or adsorb As (Beaulieu and Savage, 2005; Charlet et al., 2007; Goldberg and Glaubig, 1988; Tabelin et al., 2014b, 2017b), were abundant in the peat layers (Supplementary Fig. 5; Supplementary Table 3).

In contrast, As in sediment samples from the other four borehole cores (Ph, P-Hu, TL and TT) were partitioned mostly with the exchangeable fraction (20–49%). Arsenic in this fraction is likely associated with soluble salts (Supplementary Fig. 5) and weakly or strongly sorbed to clays/phyllosilicates and Fe-oxyhydroxides/oxides (Fig. 3; Supplementary Fig. 6). The partitioning of As in salt-like phases have also been noted in sedimentary rocks (Tabelin et al., 2012b; 2017a) while the sorption of As to clays/phyllosilicates and Fe-oxyhydroxides/oxides is well documented in the literature (Beaulieu and Savage, 2005; Fendorf et al., 1997; Garcia-Ordiales et al., 2018; Manning and Goldberg, 1996; Tabelin et al., 2013, 2014c; Waychunas et al., 1993, 2005; Yang et al., 2016). Other important As-hosting phases in the sediments of these four borehole cores include the Fe-Mn oxides (2–13%) (Supplementary Figs. 6 and 7), which are readily dissolved under reducing conditions (Stumm and Sulzberger, 1992), and the organic/sulfide fraction (2–15%) that dissociate under oxic conditions (Tabelin et al., 2017c, d).

The leachates from the sediments under oxic conditions could be divided into four groups: (i) acidic (pH < 4.5), (ii) circumneutral (pH around 6–8), (iii) weakly alkaline (pH around 8–9), and (iv) moderately alkaline (pH > 9). Acidic leachates were measured in the upper clayey silt layers (above 5 m) of LS and PT, in one of the peat layers of PT, and in the medium sand layer of TT at a depth of around 25 m (Fig. 7; Supplementary Figs. 8 and 9). Based on the characterization and leaching results, there are two possible sources of acidity in the sediments: (1) acid sulfate soils (Fig. 7; Nguyen and Itoi, 2009), (2) pyrite oxidation (Figs. 5 and 6; Park et al., 2019; Tabelin and Igarashi, 2009; Tatsuhara

et al., 2012; Tomiyama et al., 2019), and (3) decomposition of organic matter (Wang and Mulligan, 2006). Meanwhile, the slightly alkaline leachates measured in the upper clayey silt layer of Ph and P-Hu could be attributed to their considerable calcite and dolomite contents, which are known to control the pH of soil, rock and sediment systems due to their higher solubility compared with sulfide and silicate minerals (Plummer et al., 1978; Tabelin et al., 2012c, d). For the exceptionally high pH from the brownish silty clay layer of TT, one possible reason is the presence of nahcolite ($NaHCO_3$), a soluble salt sometimes found in sediments and sedimentary rocks (Sugitani et al., 2003; Tabelin et al., 2017a). This deduction is consistent with the higher Na^+ (about 50 mg/l) and HCO_3^- (about 132 mg/l) concentrations in the leachate of this sediment compared with the rest of the samples.

Dissolved As in leachates of the oxic leaching experiments (DI water) was likely dominated by arsenate (As^V) based on the Eh-pH diagram shown in Supplementary Fig. 11. Among the sediment samples, those collected from the peat layers in PT and the brownish silty clay layer in TT had the highest As leachabilities in DI water at > 0.4 mg/kg (> 44 µg/L) (Fig. 7; Supplementary Fig. 9). As discussed previously, the peat layers were rich in As-containing pyrite, organic matter, kaolinite, muscovite and clinochlore while the bulk of As in the peat layers are associated with exchangeable and organic/sulfide phases, so under acidic conditions, the release of As was likely controlled by pyrite oxidation/organic matter dissociation, proton-promoted dissolution, and adsorption-desorption reactions. Pyrite and organic matter are readily oxidized in the presence of oxygen, a process that releases their As load into solution (Kim et al., 2002; Kinsela et al., 2011; Tabelin and Igarashi 2009; Wang and Mulligan, 2006). In addition, functional groups of dissolved organic matter (DOM) like catechol are known to coordinate with metal ions like Ti^{4+}, Al^{3+} and Fe^{3+} via complexation reactions, increasing their solubility and affecting the electrochemical properties of pyrite and arsenopyrite (Li et al., 2019a, b; Park et al., 2018a). Although clays and phyllosilicates are better As adsorbents between pH 4 and 6, their sorption ability was likely depressed by the relatively high concentrations of dissolved Si and DOC, both of which are known to compete with As for sorption sites (Fig. 7; Han et al., 2013; Tabelin et al., 2018; Wang and Mulligan, 2006; Xue et al., 2019). In comparison, the brownish clayey silt layer found in TT contained only about half of As found in the peat layers (~17 mg/kg) but released similarly high amounts of As into solution (~46 µg/l), which could be attributed to

the strongly alkaline pH of the leachate (about 9.5) that enhanced not only desorption reactions of exchangeable phases but also the oxidation of As-bearing pyrite (Beaulieu and Savage, 2005; Manning and Goldberg, 1996; Tabelin and Igarashi, 2009; Tabelin et al., 2018).

To identify the factors responsible for the observed leachate chemistry when the sediments are in contact with DI water, PCA was applied to 16 parameters (pH, EC, Eh, Na^+, K^+, Mg^{2+}, Ca^{2+}, Fe, Al, dissolved Si, As, Cl^-, NO_3^-, SO_4^{2-}, HCO_3^- and DOC) of the 34 leachate samples. Three PCs had eigenvalues > 1 and they accounted for 85.8% of the total "inertia" of measured leachate chemistries (Supplementary Table 6). PC 1 (46.36%) showed high loadings of Na^+, K^+, Mg^{2+}, Fe, Al, dissolved Si, As and NO_3^-, which could infer that this principal component is related to the strong effects of clay and phyllosilicate minerals (i.e., kaolinite, muscovite and clinochlore) on the leachate chemistry including the release of As, which are consistent with our earlier deductions. PC 2 (19.4%) had high positive loadings of EC, Eh, Mg^{2+}, Ca^{2+} and SO_4^{2-} together with high negative loadings of pH. Because SO_4^{2-}, Na^+ and EC had the highest contributions to PC 2, this component could be related to the major coexisting ions controlling the EC of the leachates (Fig. 7; Supplementary Figs. 8 and 9). Meanwhile, the positive loading of Eh and negative loading of pH could be explained by the enhanced oxidation of pyrite, which makes the pH more acidic, at higher Eh values (Tabelin et al., 2018). Finally, PC 3 (14.98%) had high positive loadings of pH and HCO_3^- as well as high negative loadings of DOC and Cl^-. The high positive loadings of HCO_3^- and pH could be related to the pH control exerted by carbonate-bearing minerals, which is consistent with our earlier deduction, while the negative loadings of DOC and Cl^- could be explained by the substantial pyrite content of the organic-rich parts of the sediments and its enhanced oxidation in the presence of Cl^-, both of which lowers the HCO_3^- concentration and pH of leachates.

Acidification and reducing conditions both enhanced the release of As from all sediment samples in the six borehole cores (Fig. 4; Supplementary Figs. 3 and 4). For example, the leachability of As under reducing conditions increased by at least 30- and 50-fold in Ph and P-Hu, respectively, compared with that in DI water. The release of As in the sediments was even more dramatic under acidic conditions whereby As concentrations increased by at least 50 and 100 times in Ph and P-Hu, respectively compared with those measured in DI water (Supplementary Fig. 3). The higher

leachability of As in HCl (acidic condition) than $Na_2S_2O_4$ (reducing condition) could be attributed to two processes: (1) reducing conditions and high dissolved S concentration may induce the re-precipitation of Fe-sulfides that immobilizes a portion of dissolved As (Van Geen et al., 2004; Zheng et al., 2004), and (2) Cl^- could enhance pyrite oxidation and As release into solution via aggressively replacing surface bound hydroxyl ions to form more soluble iron-chloride complexes and suppressing the formation of a passivating sulfur-rich layer on pyrite (Lehmann et al., 2000; Park et al., 2018b).

3.3 Implications to the geochemistry of arsenic in aquifer sediments

The results of this study provide compelling evidence that the roles played by clay minerals and phyllosilicates in the release and migration of As in naturally contaminated aquifer systems are as important as those of pyrite and iron-oxyhydroxides/oxides. Although clay and phyllosilicate minerals have been recognized as important players in the mobility of As in the Ganges Delta (Acharyya et al., 2000; Charlet et al., 2007), very few studies have reported that they also play important roles in As geochemistry of groundwater in the Mekong Delta. Depending on prevailing geochemical conditions, these minerals could act as either sinks or sources of dissolved As. For example, slightly acidic pH and oxidizing conditions promote the immobilization of As via sorption reactions while under slightly alkaline conditions, they become sources of As and releases this element via desorption. Sorption-desorption reactions of As with these minerals are also strongly affected by the concentrations of coexisting ions that compete with As for adsorption sites like dissolved Si and DOC. Our results also suggest that the high SO_4^{2-} concentration of leachates from the organic-rich layers (e.g., peat layers in PT) was largely due to the dissolution of soluble salt-like phases like gypsum (e.g., the saturation index (*SI*) of gypsum from PT-6 was around -0.48) rather than the oxidation of pyrite. Finally, the reductive dissolution of As-bearing iron-oxyhydroxides was not the only process by which As could be released from sediments of the Mekong Delta. Drying-flooding/inundation cycles that promote acidification of the upper layers of the aquifer as well as Cl^--enhanced pyrite oxidation from salt-water intrusion due to the excessive abstraction of groundwater for municipal, industrial or agricultural uses could exacerbate the problem of As-contaminated groundwater in the future.

4. CONCLUSIONS

This study investigated the solid-phase partitioning of As in sediments of borehole cores collected from the Vietnamese-side of the Mekong Delta and how As is released under oxic, acidic and reducing conditions. The findings of this study are summarized as follows:

1. Substantial amounts of As were bound with the exchangeable phases, which were strongly influenced by small variations in pH and the presence of coexisting ions competing with As for adsorption sites like dissolved Si and DOC.
2. Kaolinite, muscovite and clinochlore were important sources/sinks of dissolved As depending on the pH and concentrations of coexisting ions.
3. Peat layers were found in the sediments that contained substantial amounts of As-rich framboidal and euhedral pyrite.
4. The release of As from the sediments was enhanced under acidic conditions via the dissociation of Fe-oxyhydroxides/oxides, clay minerals and phyllosilicates as well as the enhanced oxidation of pyrite due to Cl^-.
5. Arsenic mobility in the sediments was enhanced under reducing conditions via the reductive dissolution of iron-oxyhydroxides/oxides.
6. The shallow aquifer of the Mekong Delta is prone to dramatic geochemical variations due to human-induced activities and the climate/topography of the region that may enhance the release of As from sediments into the groundwater.

Acknowledgments

This study was financially supported by the Japan International Cooperation Agency (JICA) through the AUN-Seed Net Collaborative Research Program for Common Regional Issues (CRC) in ASEAN-2016. The authors also wish to thank Dr. Xinde Cao and the anonymous reviewers for their valuable inputs to this paper.

Figure Captions

FIG. 1 A map of Vietnam superimposed with the location of borehole cores used in this study.

FIG. 2 Chemical compositions of distinct lithological features in borehole cores obtained between the Hau and Tien Revers (LS and PT): (a-1) variation of major chemical components in LS with depth, (a-2) distribution of trace components (As, S, and TOC) in LS with depth, (b-1) variation of major chemical components in PT with depth, and (b-2) distribution of trace components (As, S, and TOC) in PT with depth.

FIG. 3 SEM photomicrographs and semi-quantitative point analyses of (a) clinochlore, (b) muscovite, and (c) kaolinite.

FIG. 4 Solid-phase partitioning and leaching behaviors of As with depth under various conditions: (a-1) As distribution in exchangeable, carbonate, Fe-Mn oxides (reducible), organic and sulfides, and residual phases of LS sediments, (a-2) As leachability with depth under oxidizing (DI water) conditions in LS, (a-3) As leachability with depth under acidic (HCl) and reducing ($S_2O_4^{2-}$) conditions in LS, (b-1) As distribution in exchangeable, carbonate, Fe-Mn oxides (reducible), organic and sulfides, and residual phases of PT sediments, (b-2) As leachability with depth under oxidizing (DI water) conditions in PT, (b-3) As leachability with depth under acidic (HCl) and reducing ($S_2O_4^{2-}$) conditions in PT.

FIG. 5 SEM photomicrographs of pyrite-rich organic particles in the peat layers of PT containing (a-1) framboidal pyrite with the (a-2) EDS spectra of selected areas (a-2) and (b-1) subhedral pyrite with the (b-2) EDS spectra of selected areas.

FIG. 6 SEM photomicrographs of As-bearing framboidal pyrite (a-1) and the corresponding elemental maps of As (a-2), Fe (a-3), S (a-4), O (a-5), and Si (a-6), and SEM photomicrographs of As-bearing framboidal/euhedral pyrite and Al/Fe oxyhydroxides (b-1) and the corresponding elemental maps of As (a-2), Fe (a-3), S (a-4), Al (a-5), and O (a-6).

FIG. 7 Vertical distribution of pH and coexisting ions from the leaching experiments using DI water: (a-1) pH with depth in LS, (a-2) Na^+, K^+, Fe and Al concentrations with depth in LS, (a-3) dissolved Si, SO_4^{2-}, DOC concentrations with depth in LS, (b-1) pH with depth in PT, (b-2) Na^+, K^+, Fe and Al concentrations with depth in PT, (b-3) dissolved Si, SO_4^{2-}, DOC concentrations with depth in PT.

References

Abdi, H., Williams, L.J., 2010. Principal component analysis. Wiley interdisciplinary reviews: Computational statistics 2, 433–459.

Acharyya, S.K., Lahiri, S., Raymahashay, B.C., Bhowmik, A., 2000. Arsenic toxicity of groundwater in parts of the Bengal basin in India and Bangladesh: The role of Quaternary stratigraphy and Holocene sea-level fluctuation. Environ. Geol. 39, 1127–1137.

Beaulieu, B.T., Savage, K.S., 2005. Arsenate adsorption structures on aluminum oxide and phyllosilicate mineral surfaces in smelter-impacted soils. Environ. Sci. Technol. 39, 3571–3579.

Berg, M., Stengel, C., Trang, P.T.K., Viet, P.H., Sampson, M.L., Leng, M., Samreth, S., Fredericks, D., 2007. Magnitude of arsenic pollution in the Mekong and Red River Deltas—Cambodia and Vietnam. Sci. Total Environ. 372, 413–425.

Berner, R.A., 1984. Sedimentary pyrite formation: An update. Geochim. Cosmochim. Acta 48, 605-615.

Besold, J., Biswas, A., Suess, E., Scheinost, A.C., Rossberg, A., Mikutta, C., Kretzschmar, R., Gustafsson, J.P., Planer-Friedrich, B., 2018. Monothioarsenate transformation kinetics determines arsenic sequestration by sulfhydryl groups of peat. Environ. Sci. Technol. 52, 7317–7326.

Bethke, C.M., Yeakel, S., 2011. The Geochemist's Workbench® – a User's Guide to GSS, Rxn, Act2, Tact, Spec8, React, Gtplot, X1t, X2t and Xtplot. Aqueous Solutions LLC, Urbana, Illinois.

Charlet, L., Chakraborty, S., Appelo, C.A.J., Roman-Ross, G., Nath, B., Ansari, A.A., Lanson, M., Chatterjee, D., Mallik, S.B., 2007. Chemodynamics of an arsenic “hotspot” in a West Bengal aquifer: A field and reactive transport modeling study. Appl. Geochem. 22, 1273–1292.

Clevenger, T.E., 1990. Use of sequential extraction to evaluate the heavy metals in mining wastes. Water Air Soil Poll. 50, 241–253.

Eang, K.E., Igarashi, T., Fujinaga, R., Kondo, M. and Tabelin, C.B., 2018a. Groundwater monitoring of an open-pit limestone quarry: groundwater characteristics, evolution and their connections to rock slopes. Environmen. Monit. Assess. 190(4), 193.

Eang, K.E., Igarashi, T., Kondo, M., Nakatani, T., Tabelin, C.B., Fujinaga, R., 2018b. Groundwater monitoring of an open-pit limestone quarry: Water-rock interaction and mixing estimation within the rock layers by geochemical and statistical analyses. Int. J. Min. Sci. Technol. 28, 849–857.

Feldman, P.R., Rosenboom, J.W., 2001. Cambodia drinking water quality assessment. Phnom Penh, Cambodia: World Health Organisation of the UN [WHO] in cooperation with Cambodian Ministry of Rural Development and the Ministry of Industry, Mines and Energy.

Fendorf, S., Eick, M.J., Grossl, P., Sparks, D.L., 1997. Arsenate and chromate retention mechanisms on goethite. 1. Surface structure. Environ. Sci. Technol. 31, 315–320.

Fendorf, S., Michael, H.A., Van Geen, A., 2010. Spatial and temporal variations of groundwater arsenic in South and Southeast Asia. Science, 328, 1123–1127.

Garcia-Ordiales, E., Covelli, S., Rico, J.M., Roqueñí, N., Fontolan, G., Flor-Blanco, G., Cienfuegos, P., Loredo, J., 2018. Occurrence and speciation of arsenic and mercury in estuarine sediments affected by mining activities (Asturias, northern Spain). Chemosphere 198, 281–289.

Goldberg, S., Glaubig, R.A., 1988. Anion sorption on a calcareous, montmorillonitic soil–arsenic. Soil Sci. Soc. Am. J. 52, 1297–1300.

Goldhaber, M.B., Kalan, I.R., The sulfur cycle, in: E.D. Goldberg (Ed.), The Sea, Marine Chemistry Vol. 5, Wiley-Interscience, New York, 1974, pp. 527-655.¥

Han, Y.S., Demond, A.H., Hayes, K.F., 2013. Impact of dissolved silica on arsenite removal by nano-particulate FeS and FeS-coated sand. Chemosphere 92, 477–481.

Harvey, C.F., Swartz, C.H., Badruzzaman, A.B.M., Keon-Blute, N., Yu, W., Ali, M.A., Jay, J., Beckie, R., Niedan, V., Brabander, D., Oates, P.M., 2002. Arsenic mobility and groundwater extraction in Bangladesh. Science 298, 1602–1606.

Hoang, T.H., Bang, S., Kim, K.W., Nguyen, M.H., Dang, D.M., 2010. Arsenic in groundwater and sediment in the Mekong River delta, Vietnam. Environ. Pollut. 158, 2648–2658.

Howarth, R.W., Teal, J.M., 1979. Sulfate reduction in a New England salt marsh. Limnol. Oceanogr. 24, 999–1013.

Kim, M.J., Ahn, K.H., Jung, Y., 2002. Distribution of inorganic arsenic species in mine tailings of abandoned mines from Korea. Chemosphere 49, 307–312.

Kinsela, A.S., Collins, R.N., Waite, T.D., 2011. Speciation and transport of arsenic in an acid sulfate soil-dominated catchment, eastern Australia. Chemosphere 82, 879–887.

Kocar, B.D., Polizzotto, M.L., Benner, S.G., Ying, S.C., Ung, M., Ouch, K., Samreth, S., Suy, B., Phan, K., Sampson, M., Fendorf, S., 2008. Integrated biogeochemical and hydrologic processes

driving arsenic release from shallow sediments to groundwaters of the Mekong delta. Appl. Geochem. 23, 3059–3071.

Li, X., Hiroyoshi, N., Tabelin, C.B., Naruwa, K., Harada, C., Ito, M., 2019a. Suppressive effects of ferric-catecholate complexes on pyrite oxidation. Chemosphere 214, 70-78.

Li, X., Gao, M., Hiroyoshi, N., Tabelin, C.B., Taketsugu, T., Ito, M., 2019b. Suppression of pyrite oxidation by ferric-catecholate complexes: An electrochemical study. Miner. Eng. 138, 226–237.

Manning, B.A., Goldberg, S., 1996. Modeling arsenate competitive adsorption on kaolinite, montmorillonite and illite. Clay Clay Miner. 44, 609–623.

Mar, K.K., Karnawati, D., Putra, D.P.E., Igarashi, T., Tabelin, C.B., 2013. Comparison of arsenic adsorption on lignite, bentonite, shale, and iron oxide from Indonesia. Procedia Earth Planet. Sci. 6, 242–250.

Marumo, K., Ebashi, T., Ujiie, T., 2003. Heavy metal concentrations, leachabilities and lead isotope ratios of Japanese soils. Shigen-Chishitsu 53, 125–146. [Paper in Japanese with English abstract].

Nguyen, K.P., Itoi, R., 2009. Source and release mechanism of arsenic in aquifers of the Mekong Delta, Vietnam. J. Contam. Hydrol. 103, 58–69.

Nguyen, V.L., Ta, T.K.O., Tateishi, M., 2000. Late Holocene depositional environments and coastal evolution of the Mekong River Delta, Southern Vietnam. J. Asian Earth Sci. 18, 427–439.

Park, I., Tabelin, C.B., Magaribuchi, K., Seno, K., Ito, M., Hiroyoshi, N., 2018a. Suppression of the release of arsenic from arsenopyrite by Carrier-microencapsulation using Ti-catechol complex. J. Hazard Mater. 344, 322-332.

Park, I., Tabelin, C.B., Seno, K., Jeon, S., Ito, M., Hiroyoshi, N., 2018b. Simultaneous suppression of acid mine drainage formation and arsenic release by carrier-microencapsulation using aluminum-catecholate complexes. Chemosphere 205, 414–425.

Park, I., Tabelin, C.B., Jeon, S., Li, X., Seno, K., Ito, M. and Hiroyoshi, N., 2019. A review of recent strategies for acid mine drainage prevention and mine tailings recycling. Chemosphere 219, 588–606.

Parkhurst, D.L., Appelo, C.A.J., 1999. User's guide to PHREEQC (version 2) – a computer program for speciation, batch-reactions, one-dimensional transport, and inverse geochemical calculations. U.S. Department of the Interior and U.S. Geological Survey. Water Resour. Invest. Rep. 99–4259.

511 Pham, V.N., Boyer, D., Le Mouël, J.L., Nguyen, T.K.T., 2002. Hydrogeological investigation in the
512 Mekong Delta around Ho-Chi-Minh City (South Vietnam) by electric tomography. C. R.
513 Geosci. 334, 733–740.

514 Polizzotto, M.L., Kocar, B.D., Benner, S.G., Sampson, M., Fendorf, S., 2008. Near-surface wetland
515 sediments as a source of arsenic release to ground water in Asia. Nature 454, 505.

516 Rickard, D.T., 1975. Kinetics and mechanism of pyrite formation at low temperatures. Am. J.
517 Sci. 275, 636–652.

518 Silveira, M.L., Alleoni, L.R.F., O'Connor, G.A., Chang, A.C., 2006. Heavy metal sequential
519 extraction methods – a modification for tropical soils. Chemosphere 64, 1929–1938.

520 Smedley, P.L., Kinniburgh, D.G., 2002. A review of the source, behavior, and distribution of arsenic
521 in natural waters. Appl. Geochem. 17, 517–568.

522 Stumm, W., Sulzberger, B., 1992. The cycling of iron in natural environments: Considerations based
523 on laboratory studies of heterogeneous redox processes. Geochim. Cosmochim. Acta 56, 3233–
524 3257.

525 Tabelin, C.B., Igarashi, T., 2009. Mechanisms of arsenic and lead release from hydrothermally altered
526 rock. J. Hazard. Mater. 169, 980–990.

527 Tabelin, C.B., Igarashi, T., Tamoto, S., Takahashi, R., 2012a. The roles of pyrite and calcite in the
528 mobilization of arsenic and lead from hydrothermally altered rocks excavated in Hokkaido,
529 Japan. J. Geochem. Explor. 119–120, 17–31.

530 Tabelin, C.B., Basri, A.H.M., Igarashi, T., Yoneda, T., 2012b. Removal of arsenic, boron, and
531 selenium from excavated rocks by consecutive washing. Water Air Soil Poll. 223, 4153–4167.

532 Tabelin, C.B., Igarashi, T., Takahashi, R., 2012c. Mobilization and speciation of arsenic from
533 hydrothermally altered rock in laboratory column experiments under ambient conditions. Appl.
534 Geochem. 27, 326–342.

535 Tabelin, C.B., Igarashi, T., Yoneda, T., 2012d. Mobilization and speciation of arsenic from
536 hydrothermally altered rock containing calcite and pyrite under anoxic conditions. Appl.
537 Geochem. 27, 2300–2314.

538 Tabelin, C.B., Igarashi, T., Yoneda, T., Tamamura, S., 2013. Utilization of natural and artificial
539 adsorbents in the mitigation of arsenic leached from hydrothermally altered rock. Eng. Geol. 156,
540 58–67.

Tabelin, C.B., Hashimoto, A., Igarashi, T., Yoneda, T., 2014a. Leaching of boron, arsenic and selenium from sedimentary rocks: I. Effects of contact time, mixing speed and liquid-to-solid ratio. Sci. Total Environ. 472, 620–629.

Tabelin, C.B., Hashimoto, A., Igarashi, T., Yoneda, T., 2014b. Leaching of boron, arsenic, and selenium from sedimentary rocks: II. pH dependence, speciation, and mechanisms of release. Sci. Total Environ. 473‑474, 244–253.

Tabelin, C.B., Igarashi, T., Arima, T., Sato, D., Tatsuhara, T., Tamoto, S., 2014c. Characterization and evaluation of arsenic and boron adsorption onto natural geologic materials, and their application in the disposal of excavated altered rock. Geoderma 213, 163–172.

Tabelin, C.B., Sasaki, R., Igarashi, T., Park, I., Tamoto, S., Arima, T., Ito, M., Hiroyoshi, N., 2017a. Simultaneous leaching of arsenite, arsenate, selenite, and selenate, and their migration in tunnel-excavated sedimentary rocks: I. Column experiments under intermittent and unsaturated flow. Chemosphere 186, 558–569.

Tabelin, C.B., Sasaki, R., Igarashi, T., Park, I., Tamoto, S., Arima, T., Ito, M., Hiroyoshi, N., 2017b. Simultaneous leaching of arsenite, arsenate, selenite, and selenate, and their migration in tunnel-excavated sedimentary rocks: II. Kinetic and reactive transport modeling. Chemosphere 188, 444–454.

Tabelin, C.B., Veerawattananun, S., Ito, M., Hiroyoshi, N., Igarashi, T., 2017c. Pyrite oxidation in the presence of hematite and alumina: I. Batch leaching experiments and kinetic modeling calculations. Sci. Total Environ. 580, 687–689.

Tabelin, C.B., Veerawattananun, S., Ito, M., Hiroyoshi, N., Igarashi, T., 2017d. Pyrite oxidation in the presence of hematite and alumina: II. Effects on the cathodic and anodic half-cell reactions. Sci. Total Environ. 581‑582, 126–135.

Tabelin, C.B., Igarashi, T., Villacorte-Tabelin, M., Park, I., Opiso, E.M., Ito, M., Hiroyoshi, N., 2018. Arsenic, selenium, boron, lead, cadmium, copper, and zinc in naturally contaminated rocks: A review of their sources, modes of enrichment, mechanisms of release, and mitigation strategies. Sci. Total Environ. 645, 1522–1553.

Tamoto, S., Tabelin, C.B., Igarashi, T., Ito, M., Hiroyoshi, N., 2015. Short and long term release mechanisms of arsenic, selenium and boron from tunnel-excavated sedimentary rock under in situ conditions. J. Contam. Hydrol. 175–176, 60–71.

571 Tatsuhara, T., Arima, T., Igarashi, T., & Tabelin, C. B. (2012). Combined neutralization–adsorption
572 system for the disposal of hydrothermally altered excavated rock producing acidic leachate with
573 hazardous elements. *Eng. Geol. 139*, 76-84.

574 Tessier, A., Campbell, G.C., Bisson, M., 1979. Sequential extraction procedure for the speciation of
575 particulate trace metals. Anal. Chem. 51, 844–850.

576 Tomiyama, S., Igarashi, T., Tabelin, C.B., Tangviroon, P. and Ii, H., 2019. Acid mine drainage
577 sources and hydrogeochemistry at the Yatani mine, Yamagata, Japan: A geochemical and isotopic
578 study. J. Contam. Hydrol., https://doi.org/10.1016/j.jconhyd.2019.103502

579 Van Geen, A., Rose, J., Thoral, S., Garnier, J.M., Zheng, Y., Bottero, J.Y., 2004. Decoupling of As
580 and Fe release to Bangladesh groundwater under reducing conditions. Part II: Evidence from
581 sediment incubations. Geochim. Cosmochim. Acta 68, 3475–3486.

582 Wang, S., Mulligan, C.N., 2006. Natural attenuation processes for remediation of arsenic
583 contaminated soils and groundwater. J. Hazard. Mater. B138, 459–470.

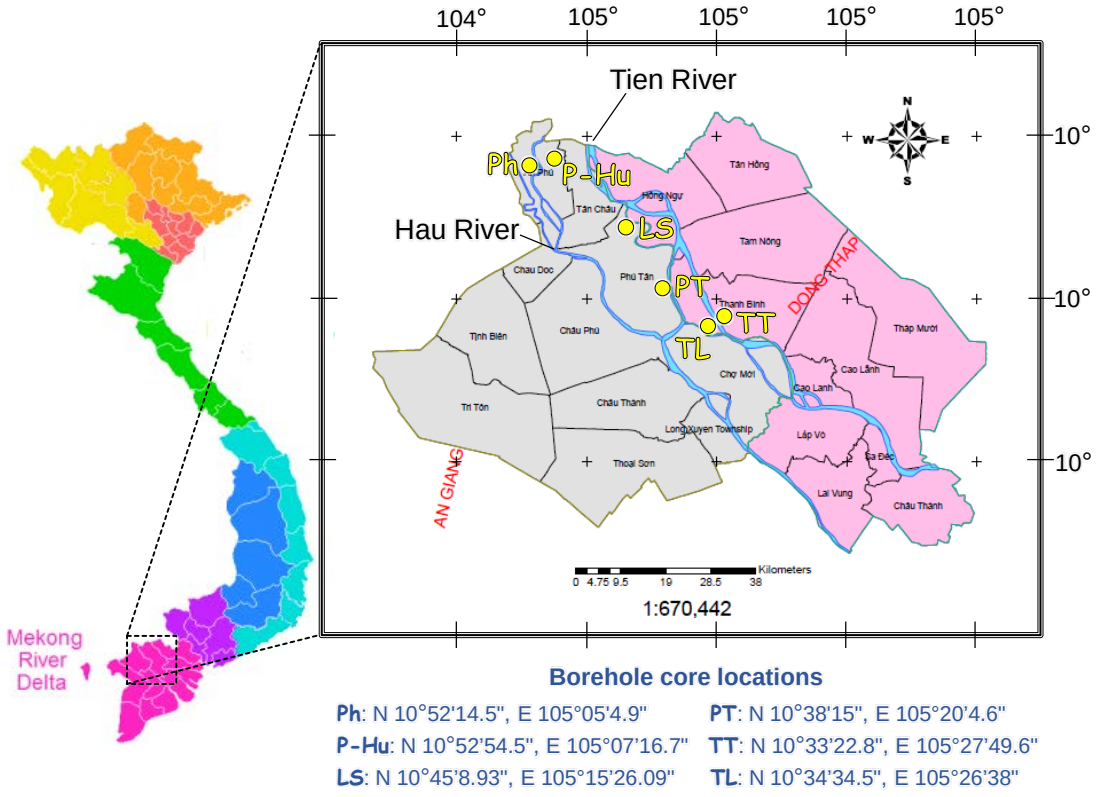
584 Waychunas, G.A., Rea, B.A., Davis, J.A., Fuller, C.C., 1993. Surface chemistry of ferrihydrite: I.
585 EXAFS studies of the geometry of coprecipitated and adsorbed arsenate. Geochim. Cosmochim.
586 Acta 57, 2251–2269.

587 Waychunas, G.A., Trainor, T., Eng, P., Catalano, J., Brown, G., Davis, J., Rogers, J., Bargar, J., 2005.
588 Surface complexation studied via combined grazing-incidence EXAFS and surface diffraction:
589 Arsenate on hematite (0001) and (1012). Anal. Bioanal. Chem. 383, 12–27.

590 Xue, Q., Ran, Y., Tan, Y., Peacock, C.L., Du, H., 2019. Arsenite and arsenate binding to ferrihydrite
591 organo-mineral coprecipitate: Implications for arsenic mobility and fate in natural
592 environments. Chemosphere 224, 103–110.

593 Yang, H.J., Lee, C.Y., Chiang, Y.J., Jean, J.S., Shau, Y.H., Takazawa, E., Jiang, W.T., 2016.
594 Distribution and hosts of arsenic in a sediment core from the Chianan Plain in SW Taiwan:
595 Implications on arsenic primary source and release mechanisms. Sci. Total Environ. 569, 212–
596 222.

597 Zheng, Y., Stute, M., Van Geen, A., Gavrieli, I., Dhar, R., Simpson, H.J., Schlosser, P., Ahmed, K.M.,
598 2004. Redox control of arsenic mobilization in Bangladesh groundwater. Appl. Geochem. 19,
599 201–214.



Borehole core locations

Ph: N 10°52'14.5", E 105°05'4.9"
P-Hu: N 10°52'54.5", E 105°07'16.7"
LS: N 10°45'8.93", E 105°15'26.09"
PT: N 10°38'15", E 105°20'4.6"
TT: N 10°33'22.8", E 105°27'49.6"
TL: N 10°34'34.5", E 105°26'38"

Figure 1

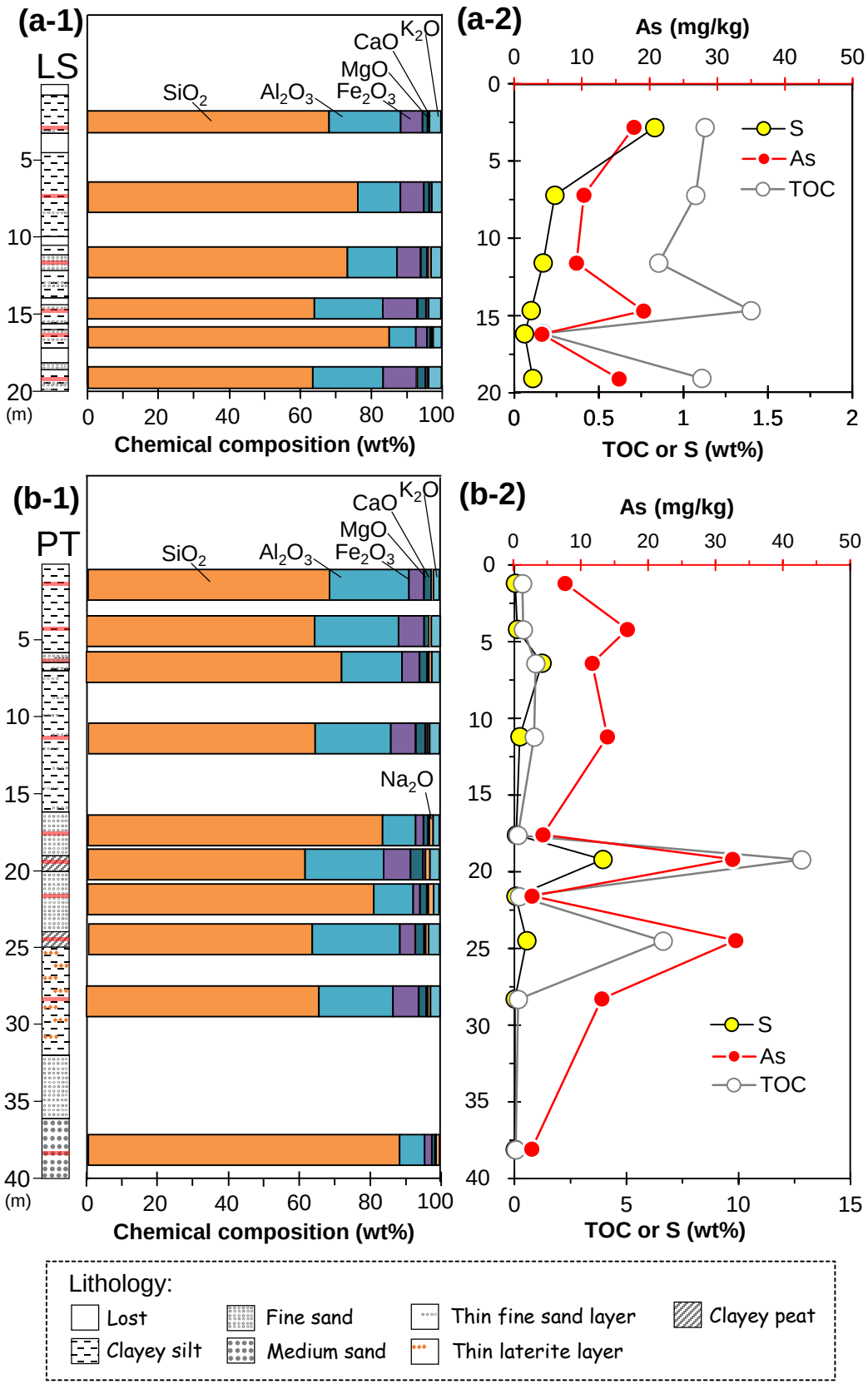

(a-1)
LS
SiO2
Al2O3
Fe2O3
MgO
CaO
K2O
(m)
Chemical composition (wt%)
(a-2)
As (mg/kg)
S
As
TOC
TOC or S (wt%)
(b-1)
PT
SiO2
Al2O3
Fe2O3
MgO
CaO
K2O
Na2O
(m)
Chemical composition (wt%)
(b-2)
As (mg/kg)
S
As
TOC
TOC or S (wt%)
Lithology:
Lost
Fine sand
Thin fine sand layer
Clayey peat
Clayey silt
Medium sand
Thin laterite layer

Figure 2

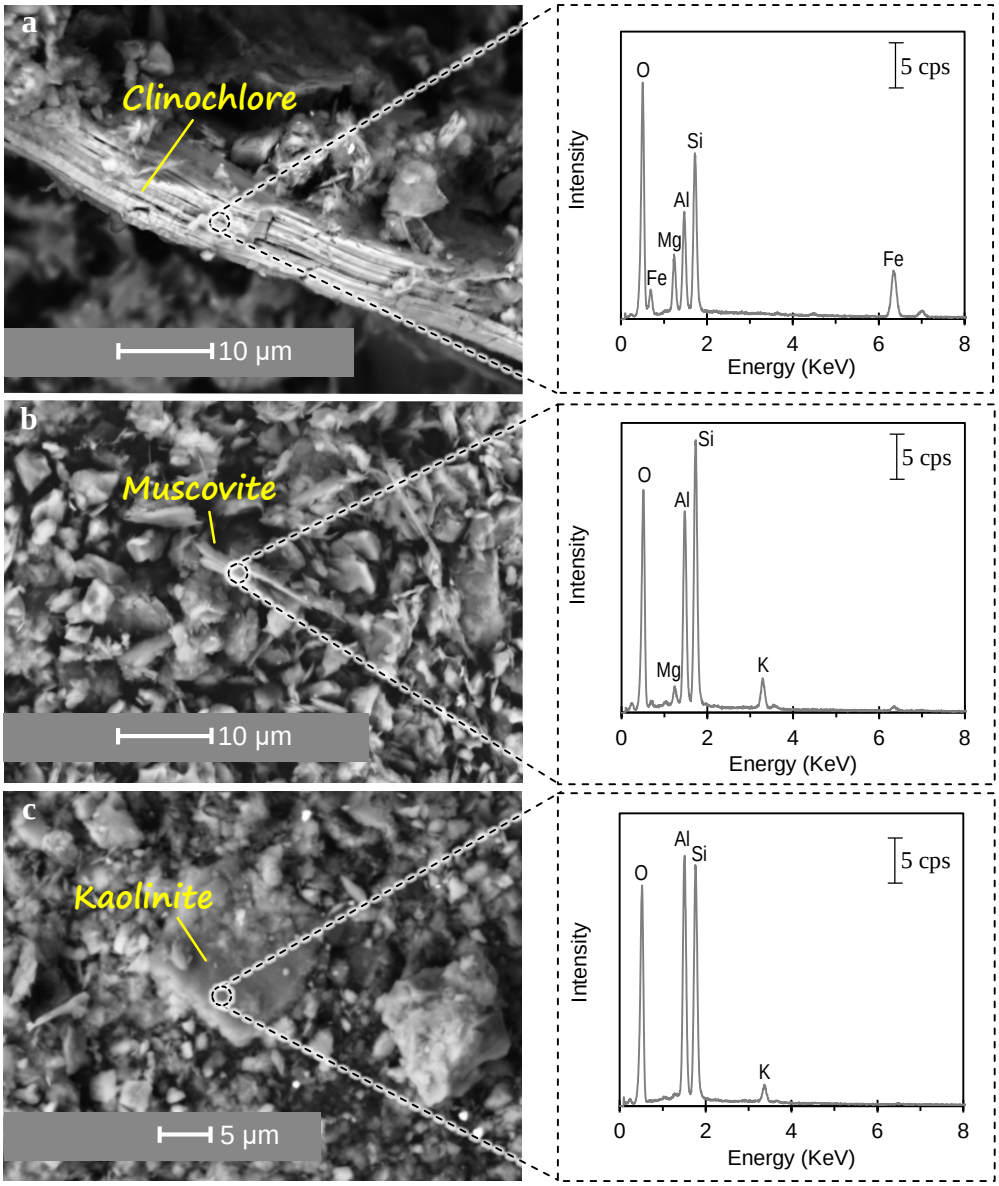

a
Clinochlore
10 µm
b
Muscovite
10 µm
c
Kaolinite
5 µm
Intensity
5 cps
O
Si
Al
Mg
Fe
K
0
2
4
6
8
Energy (KeV)

Figure 3

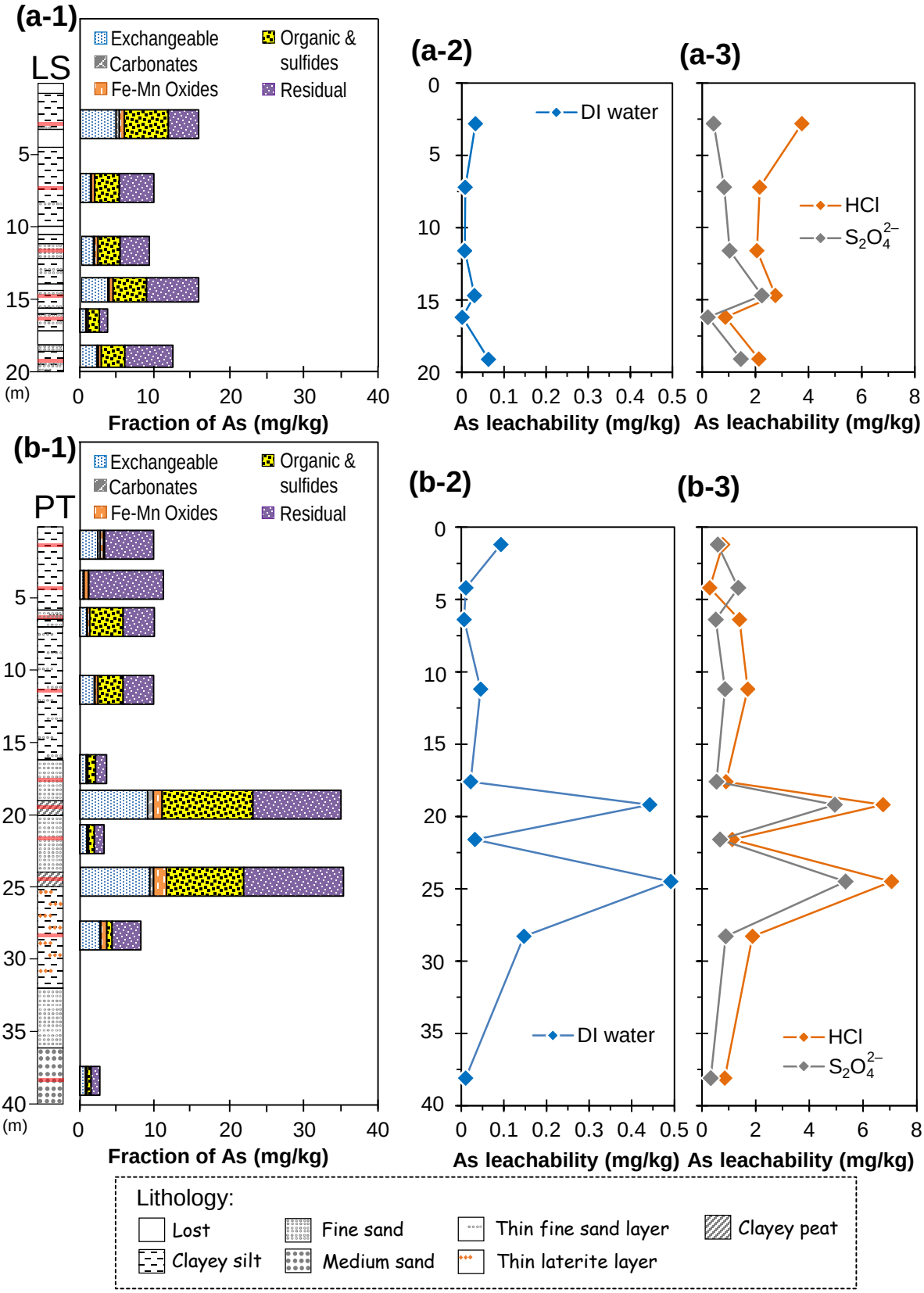

(a-1)
LS
Exchangeable
Carbonates
Fe-Mn Oxides
Organic & sulfides
Residual
(m)
Fraction of As (mg/kg)
(a-2)
DI water
As leachability (mg/kg)
(a-3)
HCl
$S_2O_4^{2-}$
As leachability (mg/kg)
(b-1)
PT
Exchangeable
Carbonates
Fe-Mn Oxides
Organic & sulfides
Residual
(m)
Fraction of As (mg/kg)
(b-2)
DI water
As leachability (mg/kg)
(b-3)
HCl
$S_2O_4^{2-}$
As leachability (mg/kg)
Lithology:
Lost
Clayey silt
Fine sand
Medium sand
Thin fine sand layer
Thin laterite layer
Clayey peat

Figure 4

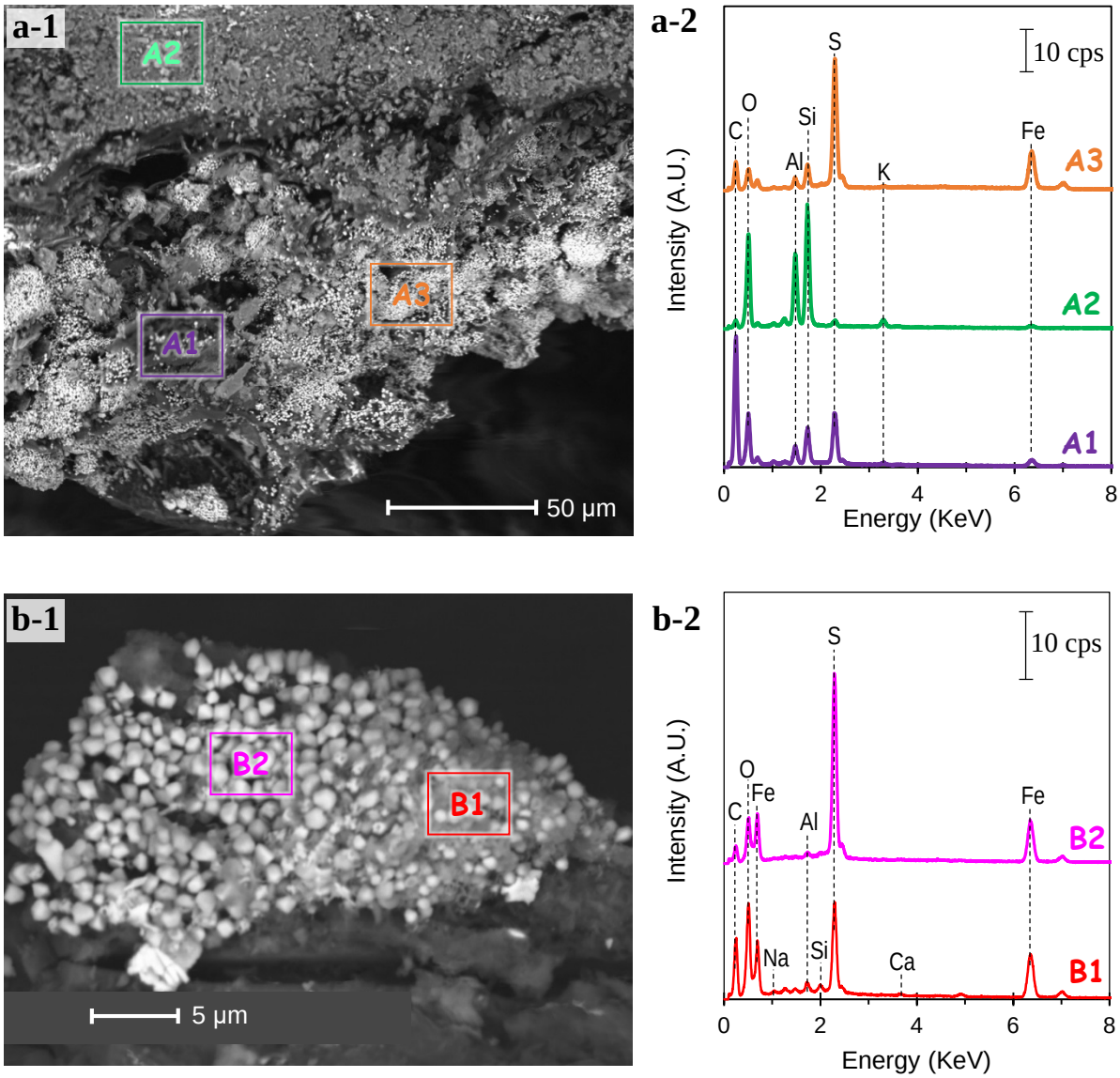

a-1
A2
A3
A1
50 μm
a-2
10 cps
S
O
C
Si
Al
K
Fe
A3
A2
A1
Intensity (A.U.)
0
2
4
6
8
Energy (KeV)
b-1
B2
B1
5 μm
b-2
10 cps
S
O
Fe
C
Al
Fe
B2
Na
Si
Ca
B1
Intensity (A.U.)
0
2
4
6
8
Energy (KeV)

Figure 5

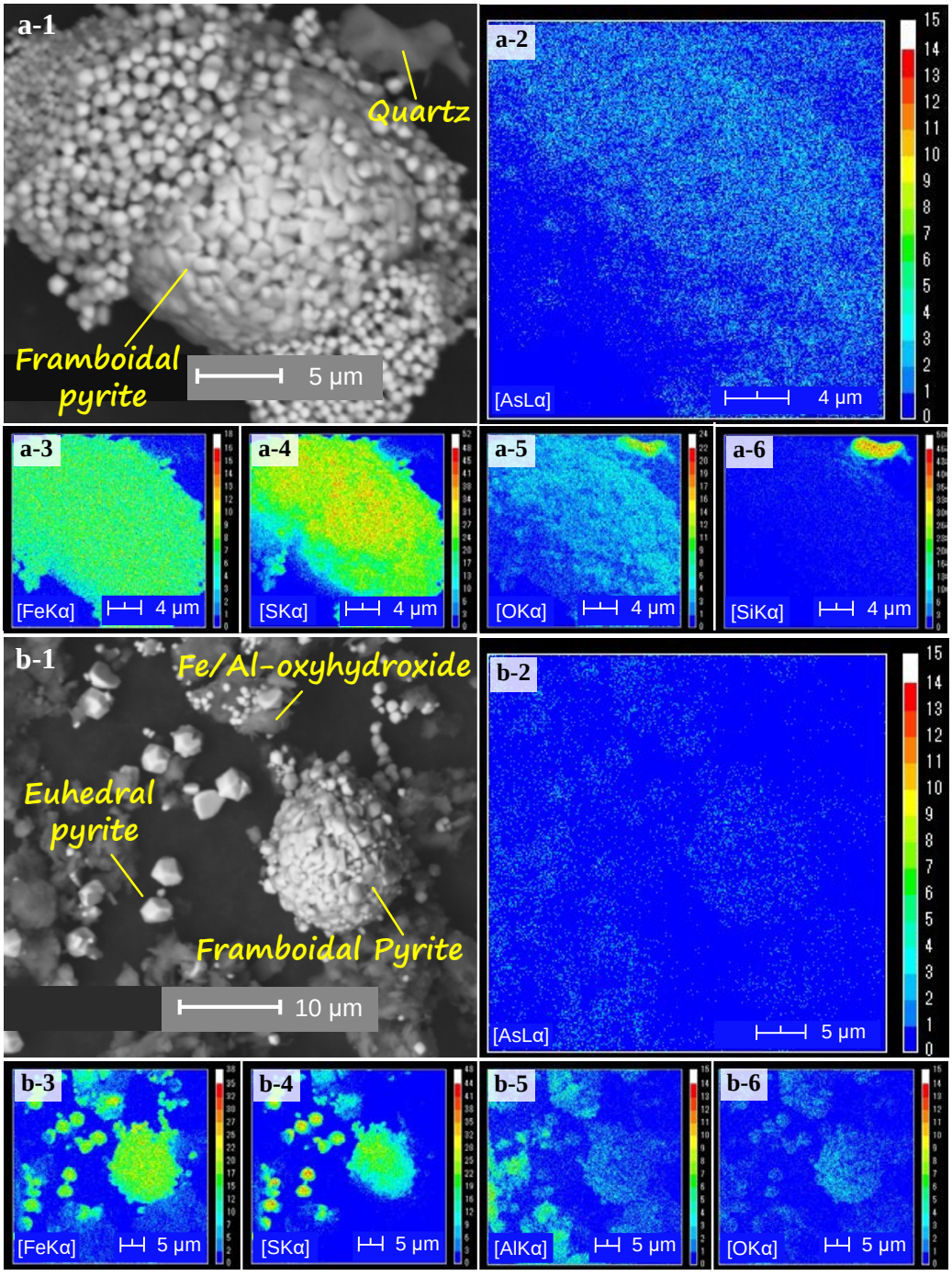

a-1
Quartz
Framboidal pyrite
5 μm
a-2
[AsLα]
4 μm
a-3
[FeKα]
4 μm
a-4
[SKα]
4 μm
a-5
[OKα]
4 μm
a-6
[SiKα]
4 μm
b-1
Fe/Al-oxyhydroxide
Euhedral pyrite
Framboidal Pyrite
10 μm
b-2
[AsLα]
5 μm
b-3
[FeKα]
5 μm
b-4
[SKα]
5 μm
b-5
[AlKα]
5 μm
b-6
[OKα]
5 μm

Figure 6

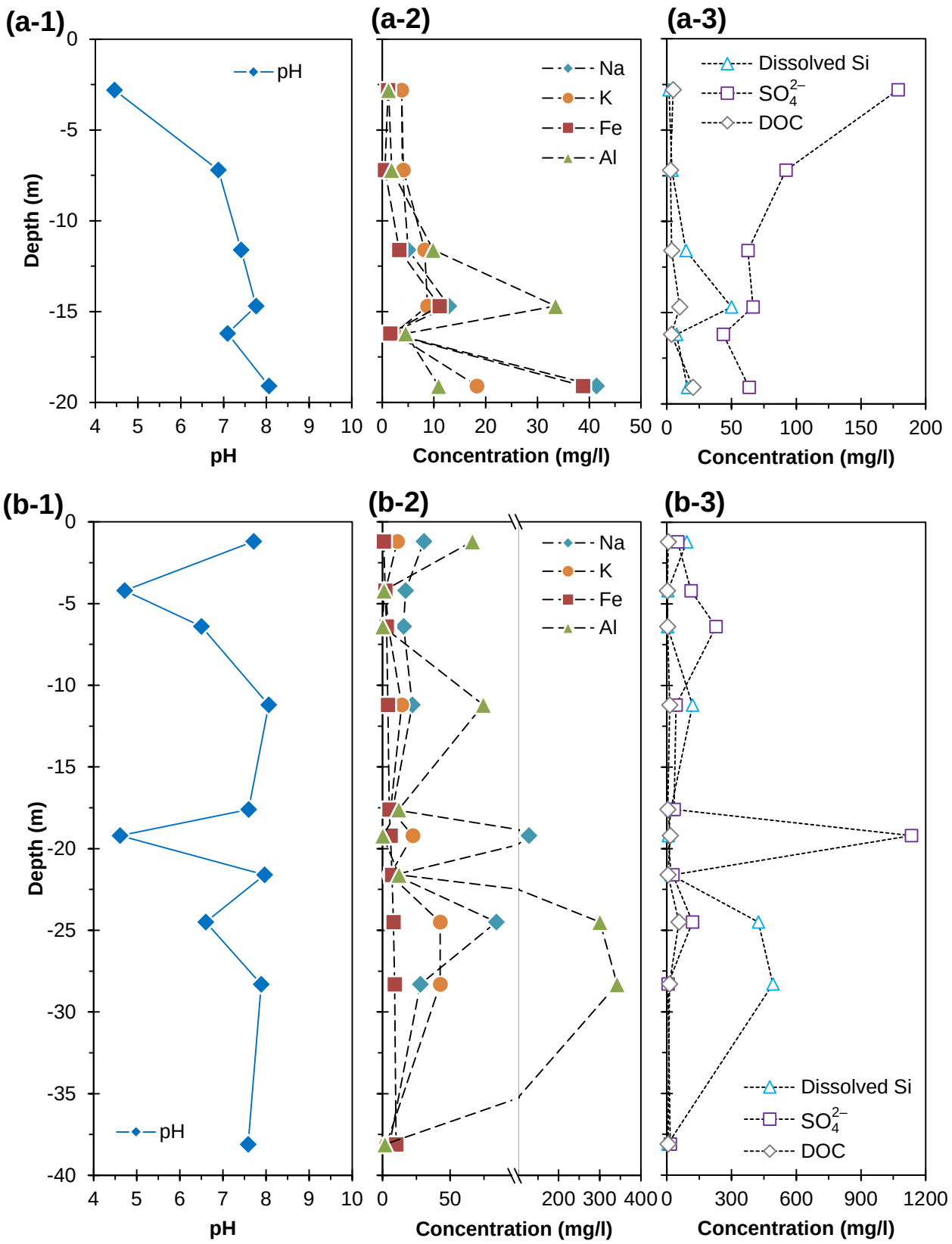

(a-1)
(a-2)
(a-3)
pH
Na
K
Fe
Al
Dissolved Si
SO4 2–
DOC
Depth (m)
pH
Concentration (mg/l)
(b-1)
(b-2)
(b-3)

Figure 7